Enhanced Water Splitting on Thin-film Hematite Photoanodes Functionalized with Lithographically Fabricated Au Nanoparticles

Beniamino Iandolo[A,B] *and Michael Zäch*[A]

[A]Department of Applied Physics, Division for Chemical Physics, Chalmers University
 of Technology, 412 96 Göteborg, Sweden.
[B]Corresponding author. Email: iandolo@chalmers.se

Iron oxide in its crystalline form (hematite, α-Fe_2O_3) is an interesting candidate as a photoanode material for photoelectrochemical cells, in spite of its non-optimal optoelectronic properties. We report here on the beneficial effect of Au nanodisks on the photocurrent of α-Fe_2O_3. Photoanodes consisting of ultra-thin α-Fe_2O_3 films lithographically functionalized with Au nanodisks of varying size were characterized and tested. We found a significant increase in photocurrent for the functionalized samples. The highest increase in incident photon-to-electron conversion efficiency is roughly one order of magnitude compared with a reference sample without Au nanodisks and was found for incident light of 420 nm in wavelength. A detailed understanding of the phenomena underlying such an increase in efficiency is crucial to fully exploit the beneficial effect of the metallic nanostructures. This would contribute to make Fe_2O_3 more competitive in the race for the development of a commercially viable device for water splitting.

Introduction

Efficient and sustainable large-scale production of chemical fuels through energy coming from the sun is an attractive option to address the global energy challenge. In particular, hydrogen has the potential to replace fossil fuels as our energy backbone in a long-term perspective.[1] Light-driven water splitting has been an appealing possibility towards clean hydrogen production ever since the pioneering work of Fujishima and Honda.[2] A distinction is typically made between molecular and photochemical (photocatalytic and photoelectrochemical (PEC)) approaches to water splitting. In the former case, light harvesting occurs in macromolecular complexes, and donor and acceptor complexes are used to separate excited electrons and holes and to run H_2 and O_2 evolution reactions with these excited charge carriers, respectively.[3,4] In the latter case, light is absorbed in a semiconductor generating electron-hole pairs. Once electrons and holes are separated, they take part in H_2 and O_2 evolution, respectively, either in close proximity to one another in the case of photocatalytic water splitting or at macroscopically different locations in a PEC cell. Intensive research is ongoing towards the development of catalysts and light absorbing materials that satisfy all the requirements – in terms of energy conversion efficiency, costs and safety – to make water splitting commercially viable.[5] Recent findings regarding all approaches mentioned above have been discussed at the Global Artificial Photosynthesis conference organized by Professor T. Faunce and held in August 2011 on Lord Howe Island, Australia.

Concerning PEC water splitting, hematite (α-Fe_2O_3) has emerged from >200 tested compounds[6] as an appealing candidate to be used as a photoanode. Fe_2O_3 is a non-toxic, inexpensive, abundant and photo-stable semiconductor capable of absorbing two thirds of the visible light owing to its bandgap of 2.0 eV.[7] However, its solar-to-chemical energy conversion efficiency remains relatively low,[8] mainly due to an intrinsic conflict between light absorption and charge transport properties. Fe_2O_3* is an n-type semiconductor characterized by poor electrical conductivity[7,8] and an extremely short hole diffusion length of around 4 nm.[9,10] This implies that only holes that are generated within a very short distance from the semiconductor-electrolyte interface avoid recombination and reach the surface where they take part into the water oxidation reaction. In contrast, the absorption of visible light in hematite requires a comparably large amount of material (the absorption length, i.e. the thickness required to absorb 63 % of the incoming light, is 118 nm for a photon with energy of 2.26 eV,[11] which corresponds to a wavelength of ~550 nm).

Metallic nanostructures have already proven to increase the performance of solid-state and dye-sensitized solar cells,[12,13] as well as the photocurrent of PEC cells.[14–16] In previous work, an enhancement in photocurrent in hematite functionalized with Au nanostructures was found in the wavelength region where such nanostructures support (localized) surface plasmon resonances, or (L)SPR. The enhanced electric fields around the nanostructures and the increased light absorption in Fe_2O_3 due to scattering by the Au were accounted for the observed changes

---

[*]The prefix is omitted hereinafter for simplicity.

in photocurrent.[15–17] However, several (other) possible mechanisms of increasing photocurrent in PEC cells upon functionalization with metallic nanostructures have been outlined in a recent review.[18]

In this Communication, we report on our observation of a significant increase in incident photon-to-current efficiency (IPCE) in Fe_2O_3 photoanodes functionalized with Au nanodisks, in a wavelength region far from the LSPR in the Au nanodisks. In particular, we tested simple and reproducible model systems based on ultra-thin Fe_2O_3 films, for which bulk electron-hole recombination is not a major limiting factor. For a detailed description of the fabrication procedure, the reader is referred to the Supplementary Material. In brief, we fabricated Fe_2O_3 films by thermal oxidation of Fe deposited by electron-beam evaporation on top of indium tin oxide (ITO)-coated glass. Then we functionalized the Fe_2O_3 films with Au nanodisks via hole-mask colloidal lithography. We focussed on Au nanodisks of various diameters, while keeping constant the disk height and surface coverage. Hole-mask colloidal lithography allows fast fabrication of random nanoparticle arrangements of various metals with different shapes in a wide size range, covering relatively large areas (i.e. a few cm^2).[19] The use of such a technique is new in this context, and is suitable for systematic studies of the influence of metallic nanoparticles due to its simplicity, tunability and versatility. We have chosen Au for our nanodisks in view of several favourable properties, including (i) proven stability under the operation conditions in a PEC cell and (ii) tunability of the LSPR peak position by appropriate choice of nanodisk size. In particular, nanodisks can be manufactured so that the LSPR peak lies in the region of poor absorption in Fe_2O_3,[20] which can be of interest in view of maximizing plasmon-related beneficial effects.

Results and Discussion

The as-fabricated iron oxide films are compact, as seen from the top-view SEM image shown in Fig. 1d, and have a roughness similar to that of the underlying 120 nm-thick ITO charge collectors (for atomic force microscopy height images, see Fig. S1 in the Supplementary Material).

All peaks in the X-ray diffraction spectra (see Fig. S2 in the Supplementary Material) can be assigned to Fe_2O_3 (JCPDS
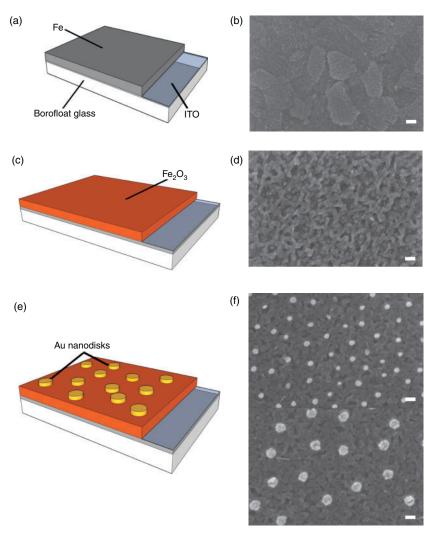

Fig. 1. Sample fabrication and imaging. Panels (a), (c) and (e) show schematic illustrations of the main preparation steps: deposition of a Fe compact thin film by electron-beam evaporation, oxidation of the Fe film into Fe_2O_3 and functionalization with Au nanodisks. Panels (b), (d) and (f) show the corresponding top-view scanning electron microscopy micrographs. The average diameter of the Au nanodisks is 50 nm in the top and 100 nm in the bottom part of panel (f). The scale bar represents 100 nm in all images.

33-0664) or ITO (JCPDS 06-0416), confirming that the films are composed of polycrystalline Fe_2O_3. One notices the presence of two preferred crystal orientations in Fe_2O_3, namely the [104] and the [110] directions, in agreement with previous studies on Fe_2O_3 thin films deposited on top of ITO.[21]

Light extinction was measured in water for the functionalized samples and for reference samples consisting of Fe_2O_3 of the respective same thickness.

Fig. 2 shows the extinction difference spectra between functionalized and non-functionalized samples, i.e. $\Delta E \equiv E_{Fe_2O_3+Au} - E_{Fe_2O_3}$. All the ΔE spectra show one peak, which corresponds to the presence of LSPR in the Au nanodisks.

Table 1 summarizes the position of the ΔE peaks for different samples. Two trends are distinguishable: first, increasing the disk diameter from 50 to 100 nm causes a redshift (i.e. shift to longer wavelengths) of the ΔE peak. In general, such a redshift is expected for increasing nanodisk diameter and is well understood in terms of dynamic depolarization of the nanodisk.[22] Second, increasing the Fe_2O_3 thickness for a given Au nanodisk diameter also results in a redshift of the ΔE peak. The change in nanoenvironment around the nanodisks accounts for the redshift; with the Fe_2O_3 thickness increasing from 25 to 40 nm, the Au disks are surrounded by a medium whose effective refractive index n_{eff} increases because Fe_2O_3 has a higher refractive index than ITO in the spectral region of interest.[23] Such an increase in n_{eff} results in the observed redshift of the ΔE peaks. Upon further increasing the Fe_2O_3 thickness to 55 nm, however, we see no further redshift. This observation can be qualitatively understood by recalling that LSPR are sensitive to changes in the refractive index of the surrounding medium only within a certain volume.[24]
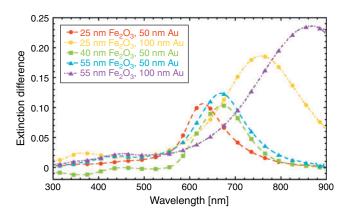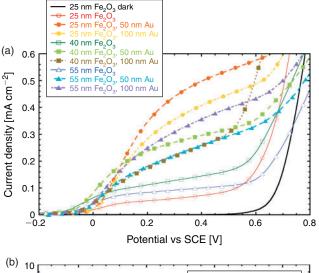
Fig. 3a shows the photocurrent – measured under white light illumination in 1 M KOH (pH 13.5) – of samples with different Fe_2O_3 thickness and Au nanodisk diameter. Further details regarding the test procedure, as well as the reproducibility of the measurements, are given in the Supplementary Material. First, we notice that the photocurrent of the bare Fe_2O_3 samples depends on the film thickness, with the 40 nm-thick film showing the highest photocurrent and lowest onset potential values (for the latter, see Fig. S3 in the Supplementary Material). Such intermediate thickness guarantees an optimal compromise between light absorption and charge transport for this film structure. This behaviour is characteristic of Fe_2O_3 compact thin films and has been observed previously.[25]

All the functionalized samples show an increase in photocurrent as compared to a bare Fe_2O_3 sample with the same thickness over the whole considered potential window. Table 2 summarizes the photocurrent increase, defined here as (photocurrent of functionalized sample – photocurrent of reference sample)/(photocurrent of reference sample), measured at 0.223 V against the saturated calomel reference electrode (which corresponds to 1.23 V against the standard hydrogen electrode at pH 13.5). The 25-nm Fe_2O_3 samples show not only the highest relative increase in photocurrent (of roughly a factor of six), but also the highest photocurrent in absolute terms. A beneficial effect of nanostructures of various metals (Au,[17] Ti[26] and even Zn[27]) on the onset potential for the photocurrent

Fig. 2. Optical extinction difference ΔE between Fe_2O_3 films functionalized with Au nanodisks of varying diameter and reference films of the same thickness without Au nanodisks.

Table 1. ΔE peak wavelength for some representative samples
Details are discussed in the text

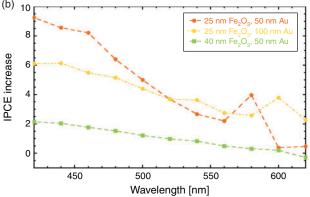| Sample	LSPR peak position λ_{LSPR} [nm]
25-nm Fe_2O_3, 50-nm Au	628
25-nm Fe_2O_3, 100-nm Au	757
40-nm Fe_2O_3, 50-nm Au	671
55-nm Fe_2O_3, 50-nm Au	669
55-nm Fe_2O_3, 100-nm Au	867

Fig. 3. Photocurrent measurements. (a) Photocurrent under white light illumination as a function of the applied potential for functionalized and reference samples. (b) Wavelength-dependent incident photon-to-electron conversion efficiency increase for selected functionalized samples.

Table 2. Summary of photocurrent increase, i.e. ($J_{Fe_2O_3+Au}$ − $J_{Fe_2O_3}$)/$J_{Fe_2O_3}$, measured under white light illumination at 1.23 V against the standard hydrogen electrode

Sample	Photocurrent increase
25-nm Fe_2O_3, 50-nm Au	5.86
25-nm Fe_2O_3, 100-nm Au	4.57
40-nm Fe_2O_3, 50-nm Au	1.13
40-nm Fe_2O_3, 100-nm Au	0.61
55-nm Fe_2O_3, 50-nm Au	1.22
55-nm Fe_2O_3, 100-nm Au	2.07

has been reported previously. Catalytic activity of the metal has then been accounted for such influence. In our case, however, we do not see a dramatic shift of the onset potential upon functionalization with Au nanodisks (see Fig. S3 in the Supplementary Material for details).

The response of the films to monochromatic light is a key to gain insight in the mechanisms responsible for the increase in photocurrent. Fig. 3b shows the increase in IPCE, defined in an analogous way as previously for the photocurrent increase, for a few representative samples.

The 25-nm Fe_2O_3 films show a higher IPCE increase than the 40-nm Fe_2O_3 film over the entire investigated wavelength range. This is consistent with the white light photocurrent-voltage measurements discussed above. We notice that the 25-nm Fe_2O_3 films are characterized by a local maximum in the IPCE increase close to the wavelength corresponding to the bandgap in Fe_2O_3. Such relative maxima are in the region of enhanced light extinction due to LSPR in the Au nanodisks. For both samples, we attribute this relative maximum in IPCE increase to the plasmonic activity of the Au nanodisks. An increase in IPCE upon functionalization with Au nanostructures in the spectral region of plasmonic activity of the Au is expected and has been recently demonstrated.[15–17] Remarkably, we observe the highest IPCE increase in our samples for the shortest wavelengths in the measurement range, between 420 and 460 nm. In this part of the visible spectrum, however, there is no clear difference in optical extinction between functionalized and reference samples. Hot electron transfer, electric field enhancement, and increased absorption due to enhanced light scattering cannot account for the observed IPCE increase in this region since plasmonic resonances are not active here. Nonetheless, we observe here the greatest improvement in IPCE, with a remarkable maximum value of 9.2 for the 25-nm hematite film functionalized with 50-nm Au disks at 420 nm. To the best of our knowledge, this is the first observation of such a pronounced effect in Fe_2O_3 films functionalized with metallic nanostructures. Considering that there is essentially no overlap with the region of increased optical extinction, we speculate that this IPCE increase is caused by a Schottky barrier at the semiconductor-metal interface that improves charge separation. The possibility of beneficial effects due to such a mechanism has been hypothesized in a recent review.[18] At present, the validity of this hypothesis is yet to be verified in our model system and is therefore the subject of current investigation.

Conclusions

In conclusion, we demonstrated that Au nanodisks deposited by hole-mask colloidal lithography enhance the photocurrent in dense, polycrystalline ultra-thin Fe_2O_3 films. The increase in

photocurrent under white light illumination is up to a factor of six for a 25-nm thin Fe_2O_3 film functionalized with 50-nm Au nanodisks. The relative maximum in IPCE increase close to the bandgap energy in Fe_2O_3 overlaps with the region of increased light extinction in the Au-functionalized samples. Therefore, we attribute such an increase in IPCE to LSPR-induced phenomena. We observed a much higher increase in IPCE for shorter wavelengths, up to an order of magnitude (for a 25-nm thin Fe_2O_3 film functionalized with 50-nm Au nanodisks), where no significant light extinction difference is caused by the Au nanodisks.

We tentatively attribute this enhancement in IPCE to a Schottky barrier at the semiconductor–metal interface, which results in improved charge separation. Further investigations are ongoing in order to verify this hypothesis. The effect of varying other parameters in this model system, such as sample geometry (for instance, Au nanodisks embedded in Fe_2O_3) and surface coverage of the Au nanodisks on the photocurrent in Fe_2O_3 should be considered. In this regard, it is worth noting that the very small surface coverage (i.e. small amount of Au) used in this work is favourable in view of issues related to availability and cost of Au. We anticipate that a combined effort in all these directions would lead to an optimized Fe_2O_3 : Au nanoparticle system where the beneficial effect of the metallic nanostructures is fully exploited. This would make Fe_2O_3 even more competitive in the race for the development of a commercially viable device for water splitting. The main competitive advantages of iron oxide as compared to molecular approaches are its low cost, its high stability, its large abundance and its potentially high solar-to-hydrogen conversion efficiency, with no need to separate hydrogen and oxygen. Iron oxide is furthermore an interesting alternative to silicon, which is currently used as photovoltaic material in Reece et al.'s artificial leaf, since it may make the device even cheaper to produce.

Supplementary Material

Details about sample fabrication and characterization (atomic force microscopy and X-ray diffraction scans) and measurements of photocurrent onset potential and of photocurrent in control samples are available on the Journal's website.

References

[1] US Department of Energy, *Basic research needs for solar energy utilization* (report) **2005**.

[2] A. Fujishima, K. Honda, *Nature* **1972**, *238*, 37. doi:10.1038/238037A0

[3] S. Y. Reece, J. A. Hamel, K. Sung, T. D. Jarvi, A. J. Esswein, J. J. H. Pijpers, D. G. Nocera, *Science* **2011**, *334*, 645. doi:10.1126/SCIENCE.1209816

[4] G. C. Dismukes, R. Brimblecombe, G. A. N. Felton, R. S. Pryadun, J. E. Sheats, L. Spiccia, G. F. Swiegers, *Acc. Chem. Res.* **2009**, *42*, 1935. doi:10.1021/AR900249X

[5] US Department of Energy, *Interim update document* (report) **2011**.

[6] F. E. Osterloh, *Chem. Mater.* **2008**, *20*, 35. doi:10.1021/CM7024203

[7] R. M. Cornell, U. Schwertmann, *The Iron Oxides* **2003** (Wiley, USA).

[8] J. A. Glasscock, P. R. F. Barnes, I. C. Plumb, A. Bendavid, P. J. Martin, *Thin Solid Films* **2008**, *516*, 1716. doi:10.1016/J.TSF.2007.05.020

[9] K. Sivula, F. Le Formal, M. Grätzel, *ChemSusChem* **2011**, *4*, 432. doi:10.1002/CSSC.201000416

[10] J. H. Kennedy, K. W. Frese, *Electrochem. Soc.* **1978**, *125*, 709. doi:10.1149/1.2131532

[11] I. Balberg, H. L. Pinch, *J. Magn. Magn. Mater.* **1978**, *7*, 12. doi:10.1016/0304-8853(78)90138-5

[12] H. A. Atwater, A. Polman, *Nat. Mater.* **2010**, *9*, 205 [and references therein]. doi:10.1038/NMAT2629

[13] S. Linic, P. Christopher, D. B. Ingram, *Nat. Mater.* **2011**, *10*, 911 [and references therein]. doi:10.1038/NMAT3151

[14] Y. Tian, T. Tatsuma, *J. Am. Chem. Soc.* **2005**, *127*, 7633.

[15] H. Gao, C. Liu, H. E. Jeong, P. Yang, *ACS Nano* **2012**, *6*, 234. doi:10.1021/NN203457A

[16] I. Thomann, B. A. Pinaud, Z. Chen, B. M. Clemens, T. F. Jaramillo, M. L. Brongersma, *Nano Lett.* **2011**, *11*, 3440. doi:10.1021/NL201908S

[17] E. Thimsen, F. Le Formal, M. Grätzel, S. C. Warren, *Nano Lett.* **2011**, *11*, 35. doi:10.1021/NL1022354

[18] S. C. Warren, E. Thimsen, *Energy, Environ. Sci.* **2012**, *5*, 5133. doi:10.1039/C1EE02875H

[19] H. Fredriksson, Y. Alaverdyan, A. Dmitriev, C. Langhammer, D. S. Sutherland, M. Zäch, B. Kasemo, *Adv. Mater.* **2007**, *19*, 4297. doi:10.1002/ADMA.200700680

[20] I. Zoric, M. Zäch, B. Kasemo, C. Langhammer, *ACS Nano* **2011**, *5*, 2535. doi:10.1021/NN102166T

[21] J. D. Desai, H. M. Pathon, S.-K. Min, K.-D. Jung, O.-S. Joo, *Semicond. Sci. Technol.* **2005**, *20*, 705. doi:10.1088/0268-1242/20/8/009

[22] K. Meier, A. Wokaun, *Opt. Lett.* **1983**, *8*, 581. doi:10.1364/OL.8.000581

[23] E. W. Palik, *Handbook of optical constants of solids* **1991** (Academic Press: USA).

[24] T. Rindzevicius, Y. Alaverdyan, W. A. Murray, W. L. Barnes, M. Käll, *J. Phys. Chem. C* **2007**, *111*, 11806. doi:10.1021/JP072564W

[25] P. Hiralal, S. Saremi-Yarahmadi, B. C. Bayer, H. Wang, S. Hofmann, K. G. Upul Wijayantha, G. A. J. Amaratunga, *Sol. Energy Mater.* **2011**, *95*, 1819. doi:10.1016/J.SOLMAT.2011.01.049

[26] A. Kleiman-Shwarsctein, M. N. Huda, A. Walsh, Y. Yan, G. D. Stucky, Y.-S. Hu, M. M. Al-Jassim, E. W. McFarland, *Chem. Mater.* **2010**, *22*, 510. doi:10.1021/CM903135J

[27] S. Kumari, A. P. Singh, C. Tripathi, D. Chauhan, S. Dass, R. Shrivastav, V. Gupta, K. Sreenivas, V. R. Satsangi, *Int. J. Phot.* **2007**, *2007*.